Preparation and Characterization of Fe_2O_3 Nanoparticles in Mesoporous Silicate

Takayuki Abe, Yukio Tachibana, Takeshi Uematsu and Masakazu Iwamoto*

Catalysis Research Center, Hokkaido University, Sapporo 060, Japan

Nanoparticles of Fe_2O_3 are encapsulated into the uniform pores of MCM-41 and the bandgap of the resulting Fe_2O_3 particles is widened from 2.1 to 4.1 eV owing to the quantum size effect.

Semiconductor nanoparticles have attracted much attention because of interest in their photochemical properties and potential applications, which are indebted to the so-called quantum size effects.[1–5] Although there are many methods to prepare the nanoparticles in glasses,[2] polymers,[3] LB films[4] and zeolites and clays,[5] one of the most important problems is how to prepare these nanoparticles with a uniform size. Another significant problem is how to maintain the properties of each nanoparticle. In recent years, a new family of molecular sieves, MCM-41, has been developed, which possess a regular hexagonal array of uniform pore openings.[6–9] The pore sizes are in the range 2–10 nm. Hence, the use of MCM-41 as a template in the preparation of nanoparticles is a route to the possible solution of above two problems. Here we report that nanoparticles of Fe_2O_3 can be encapsulated into the pores of MCM-41, and that bandgap of the resulting Fe_2O_3 particles was greatly widened owing to the quantum size effect.

The silicate MCM-41 was synthesized from a mixture of reactants with the following composition which is essentially similar to that reported in literature:[6–9] 1.00 SiO_2:0.70 dodecyltrimethylammonium ($C_{12}TMA$) chloride:0.24 NaOH:62.2 H_2O. This mixture was homogenized at room temperature by stirring. The resulting mixture was loaded into a Teflon bottle in an autoclave and statically heated at 413 K for 44 h. The resultant solid product was filtered, washed in deionized water at 353 K for 24 h, filtered and dried at 353 K. Finally, the product was calcined at 823 K for 6 h to remove the incorporated surfactant species. The properties of the MCM-41 obtained are described later.

The loading of Fe_2O_3 nanoparticles on MCM-41 was carried out by the incipient wetness method with 0.04 mol dm^{-3} aqueous iron(III) nitrate at pH 2.3. After drying in a vacuum, the resulting product was divided into two samples: before the following calcination one sample (Fe/MCM-N) was not treated further, while the other (Fe/MCM-W) was suspended in deionized water at room temperature for 1 h and again dried at 353 K. Finally, both samples were heated at a heating rate of 10 K min^{-1} in air and calcined at 973 K for 3 h. The Fe contents of both samples determined by inductively coupled plasma emission spectrometry (Perkin Elmer, Optima 3000), were 0.67 and 0.66% (*m/m*), respectively, indicating that the suspension treatment gave no change in the Fe content on MCM-41.

X-Ray powder diffraction patterns (XRD; MAC Science, MXP3), N_2 adsorption–desorption isotherms at 77 K (Quanta Chrome, Autosorb-1), transmission electron micrograph images (TEM; JEOL, JEM-1200EXII; acceleration voltage 120 kV), and diffuse reflectance ultraviolet–visible absorption spectra (UV–VIS; Shimazu, Model 2100) were measured to characterize the materials obtained.

XRD analysis was carried out to determine the structure of the materials. In the XRD pattern of the parent MCM-41, four peaks were clearly observed at 2.6, 4.5, 5.2 and 6.8°, assignable to (100), (110), (200) and (210), respectively, indexed on a hexagonal unit cell. The first intense (100) peak at 2.6° corresponds to the *d*-spacing of 3.43 nm. The XRD patterns of both samples were essentially the same as that of the parent MCM-41, but all the peaks were slightly shifted to higher 2θ by 0.06–0.16°. The results indicate that the hexagonal structure of MCM-41 was maintained throughout the incorporation treatment of Fe_2O_3, and that the lattice structure of MCM-41 was slightly shrunken by the supporting treatment. When the parent MCM-41 alone was calcined at 973 K for 3 h in air, the XRD pattern also shifted to higher 2θ by *ca.* 0.04°. Unfortunately, at the moment, the shift of the XRD peaks of Fe/MCM cannot be fully interpreted by the heating effect alone.

The pore diameters and the BET surface areas of MCM-41, determined by N_2 adsorption–desorption isotherms, were 2.26 nm and over 1000 m^2 g^{-1}, respectively, for the parent MCM-41. In the case of Fe/MCM, the pore diameter decreased by *ca.* 0.1 nm, which was consistent with the result obtained from the XRD measurements. No significant change of the BET surface area was observed because of the small amount of Fe_2O_3 loaded. TEM images of the parent MCM-41 revealed the regular hexagonal array of uniform channels with a diameter of *ca.* 2.2 ± 0.2 nm and the wall thickness of 1.2 ± 0.2 nm. The former value is in good agreement with that determined by N_2 adsorption.

We first attempted to directly observe the particles of Fe_2O_3 incorporated into the pores of MCM-41 by TEM. However, no image of Fe_2O_3 nanoparticles could be observed, probably owing to the little contrast between the pore spaces and the nano particles of Fe_2O_3. In order to confirm the presence of the Fe_2O_3 nanoparticles in the pores of MCM-41, therefore, Pt was loaded on Fe_2O_3 particles by the photodeposition technique in a $PtCl_6^{2-}$ solution.† It was confirmed in separate experiments that the photodeposition of Pt takes place on the bulk Fe_2O_3‡ and not on the parent MCM-41. Fig. 1 shows a typical top view of the Pt-loaded Fe/MCM-W. In the centre of the image, two black spots assignable to the Pt particles loaded on Fe_2O_3 nanocrystals can clearly be observed. The sizes of the Pt particles in the pores were uniform but their diameters could not be determined exactly since the sizes changed during the

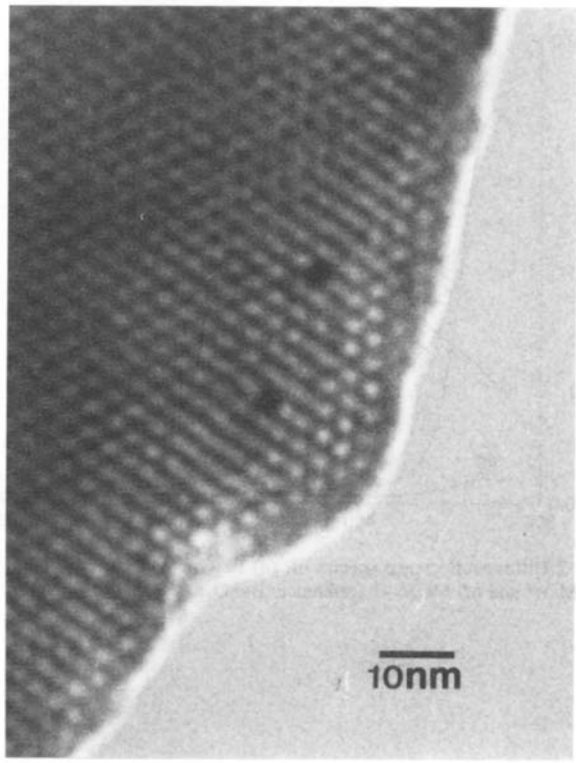

Fig. 1 TEM image of the Pt-loaded Fe/MCM-W (magnification ×1620 k)

observation of the TEM images.§ It is clear that the sizes did not exceed the sum of the pore diameter and the wall thickness. In the photographs of the side view of the Pt-loaded Fe/MCM-W, most of the Pt particles were distributed within *ca.* 100 nm of the entrance of pores. It should be noted that no Pt particle existed on the outer surface of MCM-41. In contrast, on Fe/MCM-N, not only the particles in the pores but much bigger Pt particles on the outer surface of MCM-41 were observed. It follows that the suspension treatment during the preparation of Fe/MCM-W is indispensable for migration of Fe^{III} ions loaded on the outer surface into the pores.

The UV–VIS absorption spectra of Fe/MCM-N and -W, calculated by using the Kubelka–Munk function $[F(R_\infty)]$, are shown in Fig. 2(*b*) and (*c*), respectively. The absorption spectra of a bulk Fe_2O_3 sample and MCM-41 are also depicted as (*a*) and (*d*), respectively. The parent MCM-41 gave little absorption in the range 240–800 nm. With the bulk Fe_2O_3, the direct and indirect interband transitions were observed at *ca.* 500 and 670 nm, respectively. In the absorption spectrum of Fe/MCM-N, one peak at *ca.* 250 nm and two shoulders at *ca.* 370 and 510 nm were shown. In contrast to these spectra, Fe/MCM-W yielded only one absorption band at *ca.* 250 nm. Taking the TEM observation into consideration, the bands at 370 and 510 nm are attributable to the transition in the bulk Fe_2O_3 particles on the outer surface of MCM-41, while the band at 250 nm can be assigned to that in the Fe_2O_3 nanoparticles in the pores.

The absorption edge of a UV–VIS spectrum corresponds to the bandgap of the semiconductor and can be evaluated by the plot of $[F(R_\infty)h\nu]^2$ *vs* $h\nu$ in the case of the direct interband transition.[10] The values of the bulk Fe_2O_3 and Fe/MCM-W were 2.1 and 4.1 eV, respectively. The former agreed well with the reported value of 2.2 eV.[11] These observations reveal the large shift of the bandgap of Fe_2O_3 through being loaded into the nanometer-sized pores, indicating the remarkable quantum size effect for Fe_2O_3. Although the quantum size effect for Fe_2O_3 has already been reported by a few researchers,[11,12] the change in the bandgap found in this study (2.1 to 4.1 eV) is much greater than those reported earlier. In addition, the much sharper absorption band of Fe/MCM-W shown in Fig. 2(*c*) than those in the literature indicates the quite uniform distribution of the Fe_2O_3 nanoparticles.

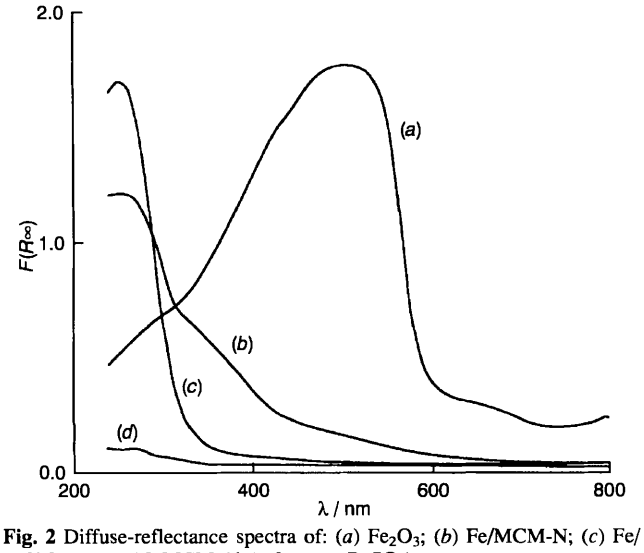

Fig. 2 Diffuse-reflectance spectra of: (*a*) Fe_2O_3; (*b*) Fe/MCM-N; (*c*) Fe/MCM-W; and (*d*) MCM-41 (reference: $BaSO_4$)

In conclusion, Fe_2O_3 nanoparticles can be prepared through encapsulation into the pores of MCM-41 and have a very wide bandgap owing to the quantum size effect. It has been proved that the bandgap of semiconductive materials can be controlled by using mesoporous materials.

This work was supported by a Grant-in-Aid for Scientific Research from the Ministry of Education, Science and Culture of Japan.

Received, 21st April 1995; Com. 5/02542G

Footnotes

† The photodeposition of Pt was carried out in a 0.01 mol dm^{-3} H_2PtCl_6 + 1% (*m/m*) MeOH solution for 30 min using a 400 W high pressure mercury lamp.[13]

‡ The bulk Fe_2O_3 sample was prepared by the thermal decomposition of iron(III) nitrate at 973 K for 3 h in air.

§ The change in the diameters of the Pt particles were due to the migration of the Pt atoms or the charging effect caused by the irradiation with the electron beam.

References

1 L. E. Brus, *J. Chem. Phys.*, 1984, **80**, 4403; R. Rossetti, R. Hull, J. M. Gibson and L. E. Brus, *J. Chem. Phys.*, 1985, **82**, 552.
2 For example: N. F. Borrelli, D. W. Hall, H. J. Holland and D. W. Smith, *J. Appl. Phys.*, 1987, **61**, 5399; E. Lifshitz, M. Yassen, L. Bykov, I. Dag and R. Chaim, *J. Phys. Chem.*, 1994, **98**, 1459.
3 For example: Y. Wang, A. Suna, W. Mahler and R. Kasowski, *J. Chem. Phys.*, 1987, **87**, 7315.
4 For example: Y. Tian, C. Wu and J. H. Fendler, *J. Phys. Chem.*, 1994, **98**, 4913.
5 For example: N. Herron, Y. Wang, M. M. Eddy, G. Stucky, D. E. Cox, K. Moller and T. Bein, *J. Am. Chem. Soc.*, 1989, **111**, 530; H. Yoneyama, S. Haga and S. Yamanaka, *J. Phys. Chem.*, 1989, **93**, 4833; A. Jentys, R. W. Grimes, J. D. Gale and C. R. A. Catlow, *J. Phys. Chem.*, 1993, **97**, 13535.
6 J. S. Beck, J. C. Vartuli, W. J. Roth, M. E. Leonowicz, C. T. Kresge, K. D. Schmitt, C. T.-W. Chu, D. H. Olson, E. W. Sheppard, S. B. McCulen, J. B. Higgins and J. L. Schlenker, *J. Am. Chem. Soc.*, 1992, **114**, 10834; J. S. Beck, J. C. Vartuli, G. J. Kennedy, C. T. Kresge, W. J. Roth and S. C. Schramm, *Chem. Mater.*, 1994, **6**, 1816; J. C. Vartuli, K. D. Schmitt, C. T. Kresge, W. J. Roth, M. E. Leonowicz, S. B. McCullen, S. D. Hellring, J. S. Beck, J. L. Schlenker, D. H. Olson and E. W. Sheppard, *Chem. Mater.*, 1994, **6**, 2317.
7 A. Monnier, F. Schuth, Q. Huo, D. Kumar, D. Margolese, R. S. Maxwell, G. D. Stucky, M. Krishnamurty, P. Petroff, A. Firouzi, M. Janicke and B. F. Chmelka, *Science*, 1993, **261**, 1299.
8 T. Yanagisawa, T. Shimizu, K. Kuroda and C. Kato, *Bull. Chem. Soc. Jpn.*, 1990, **63**, 988.
9 C.-Y. Chen, H.-X. Li and M. E. Davis, *Micropor. Mater.*, 1993, **2**, 17; C.-Y. Chen, S. L. Burkett, H.-X. Li and M. E. Davis, *Micropor. Mater.*, 1993, **2**, 27.
10 B. Karcaly and I. Hevesi, *Z. Naturforsch., Teil A*, 1971, **26**, 245.
11 H. Miyoshi and H. Yoneyama, *J. Chem. Soc., Faraday Trans. 1*, 1989, **85**, 1873.
12 J. Kiwi and M. Gratzel, *J. Chem. Soc., Faraday Trans. 1*, 1987, **83**, 1101.
13 The detailed method of the Pt photodeposition on TiO_2 was described in: D. Duonghong, E. Borgarello and M. Gratzel, *J. Am. Chem. Soc.*, 1981, **103**, 4685; S. Sato, *J. Catal.*, 1985, **92**, 11.